Received: 10 May 2019 | Revised: 15 September 2019 | Accepted: 6 October 2019

DOI: 10.1002/chir.23142

REGULAR ARTICLE

WILEY

New chiral stationary phases for liquid chromatography based on small molecules: Development, enantioresolution evaluation and chiral recognition mechanisms

Ye' Zaw Phyo[1,2] | Joana Teixeira[3] | Maria Elizabeth Tiritan[2,3,4] | Sara Cravo[2,3] | Andreia Palmeira[2,3] | Luís Gales[1,5,6] | Artur M.S. Silva[7] | Madalena M.M. Pinto[2,3] | Anake Kijjoa[1,2] | Carla Fernandes[2,3]

[1] ICBAS-Instituto de Ciências Biomédicas Abel Salazar, Universidade do Porto, Porto, Portugal

[2] Interdisciplinary Centre of Marine and Environmental Research, CIIMAR, Matosinhos, Portugal

[3] Faculdade de Farmácia, Departamento de Ciências Químicas, Laboratório de Química Orgânica e Farmacêutica, Porto, Portugal

[4] CESPU, Instituto de Investigação e Formação Avançada em Ciências e Tecnologias da Saúde (IINFACTS), Gandra, PRD, Portugal

[5] Instituto de Biologia Molecular e Celular (IBMC), Universidade do Porto, Porto, Portugal

[6] i3S – Instituto de Investigação e Inovação em Saúde, Porto, Portugal

[7] QOPNA & LAQV-REQUIMTE, Departamento de Química, Universidade de Aveiro, Aveiro, Portugal

Correspondence
Carla Fernandes, Faculdade de Farmácia, Departamento de Ciências Químicas, Laboratório de Química Orgânica e Farmacêutica, Rua de Jorge Viterbo Ferreira, 228, 4050-313 Porto, Portugal.
Email: cfernandes@ff.up.pt

Funding information
European Regional Development Fund, Grant/Award Number: PTDC/MAR-BIO/4694/2014; Fundação para a Ciência e a Tecnologia, Grant/Award Number: FCT UID/QUI/00062/2019 Strategic Funding UID/Multi/04423/2019; IINFACTS, Grant/Award Number: CHIRALBIOACTIVE-PI-3RL-IINFACTS-2019

Abstract

Recently, we reported the development of new chiral stationary phases (CSPs) for liquid chromatography (LC) based on chiral derivatives of xanthones (CDXs). Based on the most promising CDX selectors, 12 new CSPs were successfully prepared starting from suitable functionalized small molecules including xanthone and benzophenone derivatives. The chiral selectors comprising one, two, three, or four chiral moieties were covalently bonded to a chromatographic support and further packed into LC stainless-steel columns (150 × 2.1 mm I.D.). The enantioselective performance of the new CSPs was evaluated by LC using different classes of chiral compounds. Specificity for enantioseparation of some CDXs was observed in the evaluation of the new CSPs. Besides, assessment of chiral recognition mechanisms was performed by computational studies using molecular docking approach, which are in accordance with the chromatographic parameters. X-Ray analysis was used to establish a chiral selector 3D structure.

KEYWORDS

benzophenone, chiral derivative of xanthone, chiral recognition, chiral stationary phase, docking, enantioselectivity, liquid chromatography

1 | INTRODUCTION

Liquid chromatography (LC) enantioresolution using chiral stationary phases (CSPs) is one of the most significant separation approaches in academic research and industry,[1] for both analytical[2-4] and preparative purposes.[5-7] The development of CSPs for LC brought a new breath to enantioseparation processes, and nowadays, several types are available including Pirkle-type, ion-exchange-type, molecularly-imprinted, and based on

macrocyclic antibiotics, proteins, polysaccharides, cyclodextrins, crown ethers, cyclofructans, and synthetic polymers.[8,9] Among them, more than a hundred are currently commercially available.[10] Nevertheless, although many different types are described, the development of new CSPs continues to be a field of research with great importance to follow the constant challenges on different areas as well as the advances in chromatographic instrumentation.[11] Of note are the Pirkle-type CSPs that have evolved over the years, showing more progress reported, mainly due to the possibility of using a wide variety of small molecules as chiral selectors.[12,13]

Recently, we described the development of new CSPs based on chiral derivatives of xanthones (CDXs).[14] This class of small molecules is proved to be structurally promising chiral selectors for LC,[14] in addition to their broad spectrum of bioactivities.[15,16] The best enantioselectivity results were achieved for xanthone-(*R*)-(−)-α-phenylglycinol-derived CSPs.[14] In the last years, other amino alcohol-derived CSPs can be found in literature, and among them, (*R*)-phenylglycinol-derived CSPs showed good results for the LC enantioseparation of many chiral analytes.[17-20]

In this study, 12 new CSPs were successfully prepared by multistep pathways starting from suitable functionalized small molecules (xanthone and benzophenone derivatives) based on the most promising selectors (CDXs) previously reported.[14] Herein, the majority of the synthetized chiral selectors was (*R*)-phenylglycinol derivatives comprising one, two, three, or four chiral moieties and was covalently bonded through one or more sites to a chromatographic support.

Computational modeling studies by molecular docking were performed to gain the insight of structural features associated with chiral recognition mechanisms,[21,22] which not only allow the understanding the chromatographic parameters at a molecular level[23-25] but also to improve the design of new selectors.[26] These studies allowed a closer look towards the mechanisms involved in the enantiorecognition ability of this type of CSPs.

2 | MATERIALS AND METHODS

2.1 | General methods

^{1}H and ^{13}C NMR spectra were taken in DMSO-d_6 or acetone-d_6 at room temperature on a DRX-300 spectrometer. Chemical shifts are expressed in δ (ppm) values relative to TMS. ^{13}C NMR assignments were made by HSQC and HMBC experiments (long-range $J_{C\text{-}H}$ was optimized to 7 Hz). Elemental analyses were conducted on an Elemental Carlo Erba 1108 apparatus in C.A.C.T.I.–University of Vigo, Spain. HRMS mass spectra were measured on a Bruker Daltonics micrOTOF Mass Spectrometer, recorded as ESI (electrospray) mode. Melting points were obtained in a Kofler microscope and are uncorrected. The optical rotations were recorded on a Polartronic Universal polarimeter (ADP 410 polarimeter). IR spectra were recorded on a FTIR spectrometer Nicolet iS10 from Thermo Scientific with Smart OMNI-Transmission accessory (Software 188 OMNIC 8.3) in KBr. The column packing was performed in an SSI Lab Alliance–Pack in a Box, portable HPLC column packing system model CP constant pressure pump, non-flush, 0.1 to 24 mL min^{-1}, 10.000 psi, with transducer and RS-232 control, SS, 110/220 V column packer assembly (50-mL reservoir, column adapter 5/16″ 2.1 mm) Quick-Set pump control software. The empty stainless-steel columns were purchased from SSI Lab Alliance. The chiral selector loadings (μmol m^{-2}) were determined from the elemental analyses of carbon and nitrogen as follows: selector loading = $(10^6 \times \%C)/[(100 \times n \times 12) - (\%C \times Mw)]$ and selector loading = $(10^6 \times \%N)/S[(100 \times n \times 14) - (\%N \times Mw)]$, where %C and %N are the elemental analyses of carbon and nitrogen, respectively, S is the surface area, n the number of carbon or nitrogen atoms in the modified chain and Mw is the relative molecular mass.

2.2 | Chemicals and reagents

All reagents used in this study were purchased from Sigma-Aldrich Co (St Louis, Missouri) or Merck (Darmstadt, Germany). The organic solvents were obtained from Sigma-Aldrich Co (St Louis, Missouri) and were used without further purification. Silica gel 60 GF_{254} (Merck, Darmstadt, Germany) precoated plates were used for TLC. Silica gel 60 (0.04-0.063 mm, Macherey-Nagel, Düren, Germany) was used for flash column chromatography. Porous spherical silica gel Nucleosil (100 Å-5 μm, Macherey-Nagel) was used as the support material of the CSPs.

2.3 | Preparation Of CSPs 1-12

CSPs **1-12** (Figures 1 and 2) were prepared following similar synthetic procedures according to Schemes S1 to S4.

2.3.1 | Synthesis of hydroxyxanthones 1-7

The following hydroxyxanthones were synthesized according to previously described procedures.[27-33]

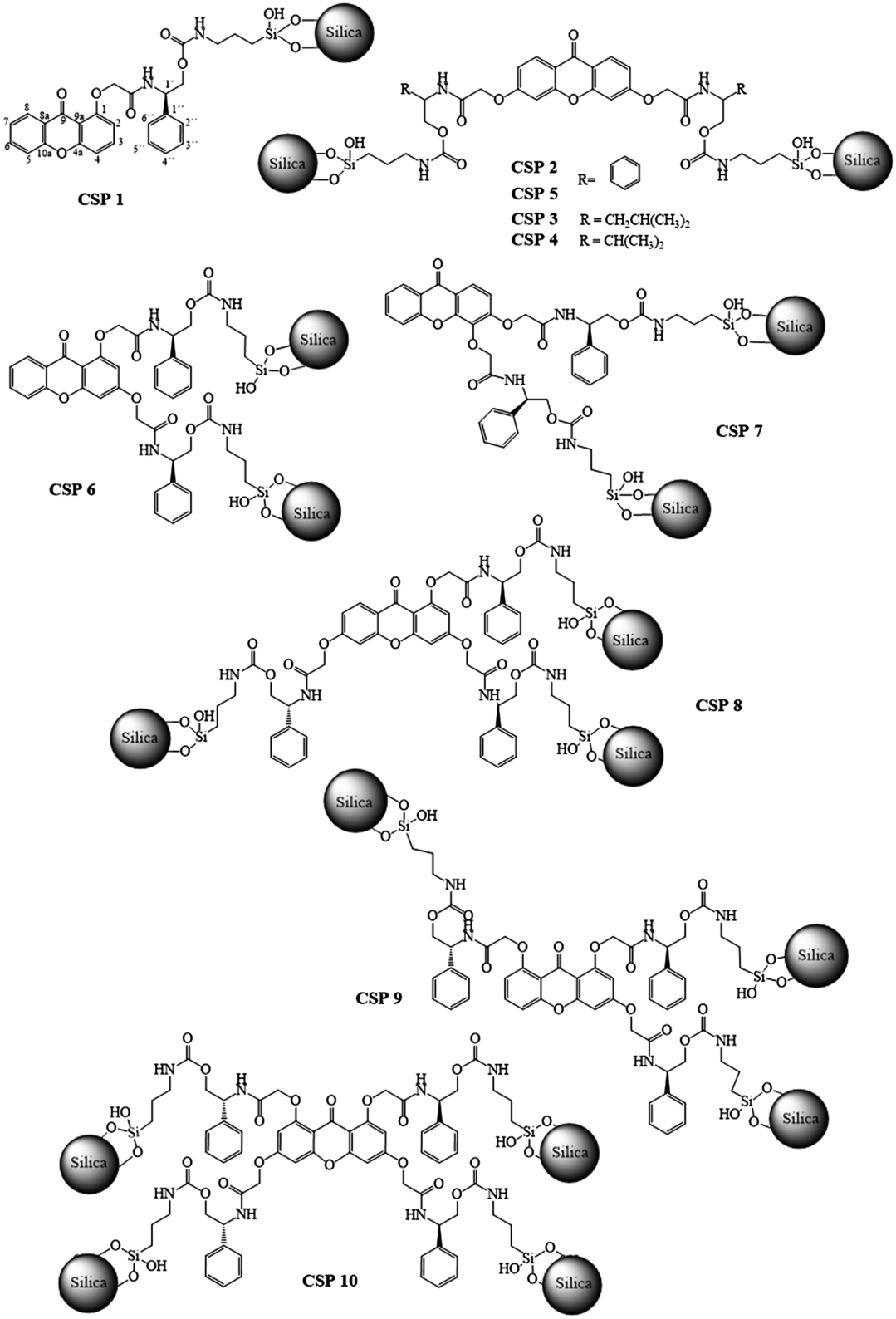

FIGURE 1 The chemical structures of CSPs based on xanthone derivatives, CSPs **1-10**

1-Hydroxy-9*H*-xanthen-9-one (**1**): Yield (51%). ^{1}H NMR and ^{13}C NMR data are shown in Supporting Information.

1,3-Dihydroxy-9*H*-xanthen-9-one (**2**): Yield (51%). ^{1}H NMR and ^{13}C NMR data are shown in Supporting Information.

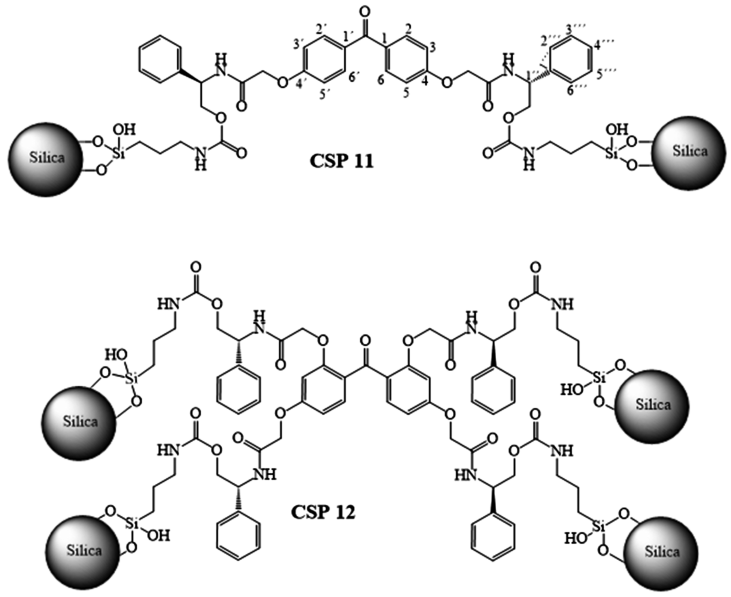

FIGURE 2 The chemical structures of CSPs based on benzophenone derivatives, CSPs **11-12**

1,3,6-Trihydroxy-9*H*-xanthen-9-one (**3**): Yield (69%). ^{1}H NMR and ^{13}C NMR data are shown in Supporting Information.

1,3,8-Trihydroxy-9*H*-xanthen-9-one (**4**): Yield (26%). ^{1}H NMR and ^{13}C NMR data are shown in Supporting Information.

1,3,6,8-Tetrahydroxy-9*H*-xanthen-9-one (**5**): Yield (24%). ^{1}H NMR and ^{13}C NMR data are shown in Supporting Information.

3,6-Dihydroxy-9*H*-xanthen-9-one (**6**): Yield (99%). ^{1}H NMR and ^{13}C NMR data are shown in Supporting Information.

3,4-Dihydroxy-9*H*-xanthen-9-one (**7**): Yield (70%). ^{1}H NMR and ^{13}C NMR data are shown in Supporting Information.

2.3.2 | Synthesis of acetate compounds 10-18

Starting from a mono-hydroxylated compound

The hydroxylated compound (**1**) (0.30 g, 1.40 mmol) was dissolved in anhydrous acetone (40 mL), and K_2CO_3 (0.58 g, 1.40 mmol) and $BrCH_2COOCH_3$ (0.2 mL, 1.70 mmol) were added. The mixture was kept under reflux and magnetic stirring for 24 hours. Afterwards, the mixture was concentrated under reduced pressure and extracted with dichloromethane (2 × 100 mL) and water (2 × 100 mL). The organic layer was evaporated under reduced pressure, and the crude product was crystallized from methanol (MeOH), to afford **10** as a white solid.

Methyl 2-[(9-oxo-9*H*-xanthen-1-yl)oxy]acetate (**10**): Yield (95%, white solid). m.p. 156°C-158°C (MeOH); ^{1}H NMR, ^{13}C NMR, and IR data are shown in Supporting Information.

Starting from a poly-hydroxylated compound

Compounds **11-18** were prepared from suitable hydroxylated compounds (**2-9**) using the same method as described for **10**, increasing the amount of K_2CO_3 and $BrCH_2COOCH_3$ according to the number of hydroxyl groups of the chemical substrate (**2-9**) and the stoichiometry of the reaction.

Dimethyl 2,2′-[(9-oxo-9*H*-xanthene-1,3-diyl)bis(oxy)] diacetate (**11**): Yield (98%, white solid). m.p. 157°C-159°C (MeOH); ^{1}H NMR, ^{13}C NMR, and IR data are shown in Supporting Information.

Trimethyl 2,2′,2″-[(9-oxo-9*H*-xanthene-1,3,6-triyl)tris (oxy)]triacetate (**12**): Yield (91%, white solid). m.p. 142°C-144°C (MeOH); ^{1}H NMR, ^{13}C NMR, and IR data are shown in Supporting Information.

Trimethyl 2,2′,2″-[(9-oxo-9*H*-xanthene-1,3,8-triyl)tris (oxy)]triacetate (**13**): Yield (93%, white solid). m.p. 151°C-153°C (MeOH); ^{1}H NMR, ^{13}C NMR, and IR data are shown in Supporting Information.

Tetramethy 2,2′,2″,2‴-[(9-oxo-9*H*-xanthene-1,3,6,8 tetrayl)tetrakis(oxy)]tetraacetate (**14**): Yield (95%, white solid). m.p. >310°C (MeOH); ^{1}H NMR, ^{13}C NMR, and IR data are shown in Supporting Information.

2,2′-[(9-Oxo-9*H*-xanthene-3,6-diyl)bis(oxy)]diacetate (**15**): Yield (88%, white solid). m.p. 228°C-230°C (MeOH); ^{1}H NMR, ^{13}C NMR, and IR data are shown in Supporting Information.

Dimethyl 2,2′-[(9-oxo-9*H*-xanthene-3,4-diyl)bis(oxy)] diacetate (**16**): Yield (95%, white solid). m.p. >310°C (MeOH); ^{1}H NMR, ^{13}C NMR, and IR data are shown in Supporting Information.

Dimethyl 2,2′-[(carbonylbis(4,1-phenylene))bis(oxy)] diacetate (**17**): Yield (94%, white solid). m.p. 175°C-177°

C (MeOH); ^{1}H NMR, ^{13}C NMR, and IR data are shown in Supporting Information.

Tetramethyl 2,2′,2″,2‴-[(carbonylbis(benzene-4,1,3-triyl))tetrakis(oxy)]tetraacetate (**18**): Yield (93%, white solid). m.p. 128°C-130°C (MeOH); ^{1}H NMR, ^{13}C NMR, and IR data are shown in Supporting Information.

2.3.3 | Synthesis of carboxylated compounds 19-27

A suitable acetate compound (1.40 mmol) was dissolved in CH_2Cl_2/MeOH (1:1 *v/v*, 100 mL) and 8M NaOH (15-30 mL) was added. The mixture was kept at room temperature and magnetic stirring for 24 hours. Afterwards, the organic solvents were evaporated under reduced pressure, and water (30 mL) was added. The aqueous phase was acidified with 5M HCl solution resulting in the formation of a precipitate that was collected by filtration under reduced pressure, washed with water, and crystallized from MeOH, to provide a carboxylated compound (**20-27**).

2-[(9-Oxo-9*H*-xanthen-1-yl)oxy]acetic acid (**19**): Yield (93%, white solid). m.p. 139°C-141°C (MeOH); ^{1}H NMR, ^{13}C NMR, and IR data are shown in Supporting Information.

2,2′-[(9-Oxo-9*H*-xanthene-1,3-diyl)bis(oxy)]diacetic acid (**20**): Yield (94%, white solid). m.p. 212°C-214°C (MeOH); ^{1}H NMR, ^{13}C NMR, and IR data are shown in Supporting Information.

2,2′,2″-[(9-Oxo-9H-xanthene-1,3,6-triyl)tris(oxy)] triacetic acid (**21**): Yield (89%, white solid). m.p. 225°C-226°C (MeOH); ^{1}H NMR, ^{13}C NMR, and IR data are shown in Supporting Information.

2,2′,2″-[(9-Oxo-9*H*-xanthene-1,3,8-triyl)tris(oxy)] triacetic acid (**22**): Yield (95%, white solid). m.p. 219°C-221°C (MeOH); ^{1}H NMR, ^{13}C NMR, and IR data are shown in Supporting Information.

2,2′,2″,2‴-[(9-Oxo-9*H*-xanthene-1,3,6,8-tetrayl)tetrakis (oxy)]tetraacetic acid (**23**): Yield (88%, white solid). m.p. >310°C (MeOH); ^{1}H NMR, ^{13}C NMR, and IR data are shown in Supporting Information.

2,2′-[(9-Oxo-9*H*-xanthene-3,6-diyl)bis(oxy)]diacetic acid (**24**): Yield (88%, yellow solid). m.p. 226°C-228°C (MeOH); ^{1}H NMR, ^{13}C NMR, and IR data are shown in Supporting Information.

2,2′-[(9-Oxo-9*H*-xanthene-3,4-diyl)bis(oxy)]diacetic acid (**25**): Yield (81%, white solid). m.p. >310°C (MeOH); ^{1}H NMR, ^{13}C NMR, and IR data are shown in Supporting Information.

2,2′-[(Carbonylbis(4,1-phenylene))bis(oxy)]diacetic acid (**26**): Yield (88%, white solid). m.p. 234°C-236°C (MeOH); ^{1}H NMR, ^{13}C NMR, and IR data are shown in Supporting Information.

2,2′,2″,2‴-[(Carbonylbis(benzene-4,1,3-triyl))tetrakis (oxy)]tetraacetic acid (**27**): Yield (80%, white solid). m.p. 232°C-235°C (MeOH); ^{1}H NMR, ^{13}C NMR, and IR data are shown in Supporting Information.

2.3.4 | Synthesis of chiral selectors 28-39

Starting from a monocarboxylated compound

The carboxylated compound **19** (0.25 g, 0.93 mmol) was dissolved in tetrahydrofuran (THF, 50 mL), and triethylamine (TEA, 380 μL, 2.66 mmol) was added. Then *O*-(benzotriazol-1-yl)-*N*,*N*,*N*′,*N*′-tetramethyluronium tetrafluoroborate (TBTU, 0.37 g, 1.11 mmol) and (*R*)-(−)-α-phenylglycinol (0.16 g, 1.11 mmol) were added. The mixture was stirred at room temperature for 5 hours. The solvent was evaporated under reduced pressure, and the crude product was dissolved in $CHCl_3$ (100 mL). This solution was washed with 1M HCl (2 × 50 mL), saturated solution of $NaHCO_3$ (2 × 50 mL), and water (3 × 50 mL). The organic layer was dried with anhydrous sodium sulphate and filtered, and the solvent was evaporated under reduced pressure. The crude product was recrystallized from $CHCl_3$/MeOH to afford **28**.

(*R*)-*N*-(2-Hydroxy-1-phenylethyl)-2-[(9-oxo-9*H*-xanthen-1-yl)oxy]acetamide (**28**): Yield (86%, white solid). m.p. 168°C-170°C ($CHCl_3$:MeOH); $[\alpha]_D^{25°C}$ −219.0 ($c = 0.32 \times 10^{-3}$ g mL^{-1} in $CHCl_3$); ^{1}H NMR, ^{13}C NMR, IR, and HRMS data are shown in Supporting Information; e.r. >99% (LC; Column: (*S*,*S*)-Whelk-O1 (25 cm × 4.6 mm I.D., 5-μm particle size), mobile phase: MeOH/CH_3CN (50:50 v:v), 1.0 mL min^{-1}, λ_{max} 254 nm, k_1: 0.63, k_2: 0.85). The structure of compound **28** was determined by X-ray crystallography (Section 2.4).

Starting from polycarboxylated compounds

Compounds **29-39** were prepared from suitable carboxylated compounds (**20-27**) using the same method as described for **19**, increasing the amount of TEA, TBTU, and appropriate chiral reagent according to the number of carboxylic groups of the chemical substrates (**20-27**) and the stoichiometry of the reaction.

2,2′-{[9-Oxo-9*H*-xanthene-1,3-diyl)bis(oxy)]bis[*N*-((*R*)-2-hydroxy-1 phenylethyl]acetamide]} (**29**): Yield (85%, white solid). m.p.: 154°C-156°C ($CHCl_3$:MeOH); $[\alpha]_D^{25°C}$ −300.0 ($c = 0.1 \times 10^{-3}$ g mL^{-1} in $CHCl_3$); ^{1}H NMR, ^{13}C NMR, IR, and HRMS data are shown in Supporting Information; e.r. >99% (LC; Column: (*S*,*S*)-Whelk-O1 (25 cm × 4.6 mm I.D., 5-μm particle size), mobile phase: MeOH/CH_3CN (50:50 v:v), 1.0 mL min^{-1}, λ_{max} 254 nm, k_1: 0.61, k_2: 1.33).

2,2′,2″-{[9-Oxo-9*H*-xanthene-1,3,6-triyl)tris(oxy)]tris [*N*-(*R*)-2-hydroxy-1-phenylethyl]acetamide} (**30**): Yield (88%, white solid). m.p.: 163°C-165°C ($CHCl_3$:MeOH);

$[\alpha]_D^{25°C}$ −285.0 ($c = 0.21 \times 10^{-3}$ g mL^{-1} in $CHCl_3$); ^{1}H NMR, ^{13}C NMR, IR, and HRMS data are shown in Supporting Information; e.r. >99% (LC; Column: (*S*,*S*)-Whelk-O1 (25 cm × 4.6 mm I.D., 5-μm particle size), mobile phase: MeOH/CH_3CN (50:50 v:v), 1.0 mL min^{-1}, λ_{max} 254 nm, k_1: 0.63, k_2: 1.90).

2,2′,2″-{[9-Oxo-9*H*-xanthene-1,3,8-triyl)tris(oxy)]tris [*N*-(*R*)-2-hydroxy-1-phenylethyl]acetamide} (**31**): Yield (90%, white solid). m.p. 133°C-136°C ($CHCl_3$:MeOH); $[\alpha]_D^{25°C}$ −300.0 ($c = 0.1 \times 10^{-3}$ g mL^{-1} in $CHCl_3$); ^{1}H NMR, ^{13}C NMR, IR, and HRMS data are shown in Supporting Information; e.r. >99% (LC; Column: (*S*,*S*)-Whelk-O1 (25 cm × 4.6 mm I.D., 5-μm particle size), mobile phase: MeOH/CH_3CN (50:50 v:v), 1.0 mL min^{-1}, λ_{max} 254 nm, k_1: 0.60, k_2: 2.49).

2,2′,2″,2‴-{[(9-Oxo-9*H*-xanthene-1,3,6,8-tetrayl) tetrakis(oxy)]tetrakis[*N*-(*R*)-2-hydroxy-1-phenylethyl] acetamide} (**32**): Yield (78%, white solid). m.p. >350° C ($CHCl_3$:MeOH); $[\alpha]_D^{25°C}$ −308.0 ($c = 0.13 \times 10^{-3}$ g mL^{-1} in $CHCl_3$); ^{1}H NMR, ^{13}C NMR, IR, and HRMS data are shown in Supporting Information; e.r. > 99% (LC; Column: (*S*,*S*)-Whelk-O1 (25 cm × 4.6 mm I.D., 5-μm particle size), mobile phase: MeOH/CH_3CN (50:50 v:v), 1.0 mL min^{-1}, λ_{max} 254 nm, k_1: 0.42, k_2: 0.62).

2,2′-{[(9-Oxo-9*H*-xanthene-3,6-diyl)bis(oxy)]bis[*N*-(*S*)-2-hydroxy-1-phenylethyl]acetamide} (**33**): Yield (80%, white solid). m.p. 178°C-180°C ($CHCl_3$:MeOH); $[\alpha]_D^{25°C}$ +455.0 ($c = 0.088 \times 10^{-3}$ g mL^{-1} in $CHCl_3$); ^{1}H NMR, ^{13}C NMR, IR, and HRMS data are shown in Supporting Information; e.r. >99% (LC; Column: (*S*,*S*)-Whelk-O1 (25 cm × 4.6 mm I.D., 5-μm particle size), mobile phase: MeOH/CH_3CN (50:50 v:v), 1.0 mL min^{-1}, λ_{max} 254 nm, k_1: 0.72, k_2: 1.77).

2,2′-{[(9-Oxo-9*H*-xanthene-3,6-diyl)bis(oxy)]bis[*N*-(*S*)-1-hydroxy-4-methylpentan-2-yl]acetamide} (**34**): Yield (80%, white solid). m.p. 228°C-230°C ($CHCl_3$:MeOH); $[\alpha]_D^{25°C}$ +400.0 ($c = 0.12 \times 10^{-3}$ g mL^{-1} in CH_3CN); ^{1}H NMR, ^{13}C NMR, IR, and HRMS data are shown in Supporting Information; e.r. >99% (LC; Column: Lux celullose-2 (15 cm × 4.6 mm I.D., 3-μm particle size), mobile phase: 100% EtOH, 0.5 mL min^{-1}, λ_{max} 254 nm, k_1: 1.34, k_2: 2.90).

2,2′-{[(9-Oxo-9*H*-xanthene-3,6-diyl)bis(oxy)]bis[*N*-(*S*)-1-hydroxy-3-methylbutan-2-yl]acetamide} (**35**): Yield (80%, white solid). m.p. 236°C-238°C ($CHCl_3$:MeOH); $[\alpha]_D^{25°C}$ +417.0 ($c = 0.12 \times 10^{-3}$ g mL^{-1} in CH_3CN); ^{1}H NMR, ^{13}C NMR, IR, and HRMS data are shown in Supporting Information; e.r. >99% (LC; Column: Lux celullose-2 (15 cm × 4.6 mm I.D., 3-μm particle size), mobile phase: 100% EtOH, 0.5 mL min^{-1}, λ_{max} 254 nm, k_1: 1.55, k_2: 2.89).

2,2′-{[(9-Oxo-9*H*-xanthene-3,6-diyl)bis(oxy)]bis[*N*-(*R*)-2-hydroxy-1-phenylethyl]acetamide} (**36**): Yield (85%, white solid). m.p. 177°C-179°C ($CHCl_3$:MeOH); $[\alpha]_D^{25°C}$ −455.0 ($c = 0.088 \times 10^{-3}$ g mL^{-1} in $CHCl_3$); ^{1}H NMR, ^{13}C NMR, IR, and HRMS data are shown in Supporting Information; e.r. >99% (LC; Column: (*S*,*S*)-Whelk-O1 (25 cm × 4.6 mm I.D., 5-μm particle size), mobile phase: MeOH/CH_3CN (50:50 v:v), 1.0 mL min^{-1}, λ_{max} 254 nm, k_1: 0.72, k_2: 1.77).

2,2′-{[(9-Oxo-9*H*-xanthene-3,4-diyl)bis(oxy)]bis[*N*-(*R*)-2-hydroxy-1-phenylethyl]acetamide} (**37**): Yield (57%, white solid). m.p. 202°C-204°C ($CHCl_3$:MeOH); $[\alpha]_D^{25°C}$ −300.0 ($c = 0.1 \times 10^{-3}$ g mL^{-1} in $CHCl_3$); ^{1}H NMR, ^{13}C NMR, IR, and HRMS data are shown in Supporting Information; e.r. >99% (LC; Column: (*S*,*S*)-Whelk-O1 (25 cm × 4.6 mm I.D., 5-μm particle size), mobile phase: MeOH/CH_3CN (50:50 v:v), 1.0 mL min^{-1}, λ_{max} 254 nm, k_1: 0.53, k_2: 1.21).

2,2′-{[(Carbonylbis(4,1-phenylene)bis(oxy)]bis[*N*-(*R*)-2-hydroxy-1-phenylethyl]acetamide} (**38**): Yield (86%, white solid). m.p. 173°C-175°C ($CHCl_3$:MeOH); $[\alpha]_D^{25°C}$ −238.0 ($c = 0.21 \times 10^{-3}$ g mL^{-1} in $CHCl_3$); ^{1}H NMR, ^{13}C NMR, IR, and HRMS data are shown in Supporting Information; e.r. >99% (LC; Column: (*S*,*S*)-Whelk-O1 (25 cm × 4.6 mm I.D., 5-μm particle size), mobile phase: MeOH/CH_3CN (50:50 v:v), 1.0 mL min^{-1}, λ_{max} 254 nm, k_1: 0.43, k_2: 0.77).

2,2′,2″,2‴-{[(Carbonylbis (benzene-4,1,3-triyl)tetrakis (oxy)]tetrakis[*N*-(*R*)-2-hydroxy-1-phenylethyl]acetamide} (**39**): Yield (79%, white solid). m.p. >350°C ($CHCl_3$: MeOH); $[\alpha]_D^{25°C}$ −333.0 ($c = 0.12 \times 10^{-3}$ g mL^{-1} in $CHCl_3$); ^{1}H NMR, ^{13}C NMR, IR, and HRMS data are shown in Supporting Information; e.r. >99% (LC; Column: (*S*,*S*)-Whelk-O1 (25 cm × 4.6 mm I.D., 5-μm particle size), mobile phase: MeOH/CH_3CN (50:50 v:v), 1.0 mL min^{-1}, λ_{max} 254 nm, k_1: 0.39, k_2: 0.62).

2.3.5 | Synthesis and covalent linkage of silylated selectors onto the silica gel

Starting from a selector with one chiral unit

The chiral compound **28** (0.51 mmol) was dissolved in anhydrous toluene (20 mL), and TEA (108 μL, 1.51 mmol) and 3-(triethoxysilyl)propylisocyanate (200 μL, 1.51 mmol) were added. The mixture was refluxed for 72 hours. The solvent was evaporated under reduced pressure, and the crude product was dissolved in anhydrous toluene (30 mL). Silica gel Nucleosil (800 mg, 100 Å-5 μm, Macherey-Nagel) previously dried, in a desiccator under vacuum with phosphorus pentoxide for 24 hours, was suspended in the same solvent (30 mL). Following, the crude product solution was added. The reaction mixture was gently stirred at reflux for 72 hours. The modified silica was filtered and washed successively with toluene, MeOH, acetone, ethyl acetate,

dichloromethane, and *n*-hexane (100 mL). The bonded phase was dried in a desiccator under vacuum for 24 hours, affording the CSP.

Starting from a selector with more than one chiral unit

The silylation reaction of selectors with more than one chiral unit (**29-39**) was performed using the same conditions as described for selector **28**, increasing the amount of TEA and 3-(triethoxysilyl)propylisocyanate, according to the number of chiral units of the selector (**29-39**) and the stoichiometry of the reaction. In some cases, anhydrous CH_3CN (**34-36**, **39**) or anhydrous CH_3CN with few drops of DMSO (**29**, **33**) or anhydrous toluene with few drops of THF and DMSO (**30**) were used due to the low solubility of selectors. The covalent linkage of silylated selectors onto the silica gel was performed using the same method as described for **28**. Elemental analyses were performed to compare the extent of covalent binding of each chiral selector to silica. The chiral selector loadings ($\mu mol/m^2$) were determined from the elemental analyses of carbon and nitrogen (Table 1).

TABLE 1 Elemental analysis and chiral selector loadings for CSPs **1-12**

	Elemental analysis				
	%C	%N	%H	% selector loading (based on C), μ mol m^{-2}	% selector loading (based on N), μ mol m^{-2}
CSP **1**	18.21	2.91	1.99	2.32	6.94
CSP **2**	13.49	2.21	1.99	1.03	1.75
CSP **3**	13.66	2.26	2.13	1.22	1.77
CSP **4**	7.58	0.98	1.29	0.61	0.59
CSP **5**	18.84	4.21	2.91	1.67	6.72
CSP **6**	21.63	4.37	2.44	2.09	7.59
CSP **7**	13.11	2.55	2.02	1.00	2.21
CSP **8**	23.66	5.95	3.91	1.87	18.7
CSP **9**	6.15	0.91	1.21	0.30	0.36
CSP **10**	14.06	2.19	3.06	0.67	0.82
CSP **11**	14.81	2.19	2.19	1.18	1.71
CSP **12**	9.13	1.15	1.33	0.38	0.35

2.3.6 | LC column packing

Each packing material (approximately 1.0 g) was sieved, slurried in Hex: 2-PrOH (50:50 *v*/v) (50 mL), and sonicated for 3 minutes. Then the suspension was poured into the chamber of a column packer and packed into a stainless-steel column (150 × 2.1 mm I.D.) using Hex: 2-PrOH (90:10 v/v) as a packing solvent, under a pressure no more than 6000 psi.

2.4 | X-ray crystallography

A single crystal of (*R*)-*N*-(2-hydroxy-1-phenylethyl)-2-[(9-oxo-9*H*-xanthen-1-yl)oxy]acetamide (**28**) was mounted on a cryoloop using paratone. X-ray diffraction data were collected at 290 K with a Gemini PX Ultra equipped with CuK_α radiation (λ = 1.54184 Å). The structure was solved by direct methods using SHELXS-97 and refined with SHELXL-97.[34] Crystal was orthorhombic, space group $P2_12_12_1$, cell volume 3820.8(3) $Å^3$, and unit cell dimensions a = 8.3606(3) Å, b = 8.9346(3) Å, and c = 51.149(3) Å (uncertainties in parentheses). There were two molecules in the asymmetric unit, one of them with an oxygen atom with alternate conformation. Non-hydrogen atoms were refined anisotropically. Hydrogen atoms were either placed at their idealized positions using appropriate HFIX instructions in SHELXL and included in subsequent refinement cycles or were directly found from difference Fourier maps and were refined freely with isotropic displacement parameters. The flack x parameter was refined with SHELXL-97 by means of TWIN and BASF to yield 0.097(3). The refinement converged to R (all data) = 8.44% and wR2 (all data) = 12.14%.

Full details of the data collection and refinement and tables of atomic coordinates, bond lengths and angles, and torsion angles have been deposited with the Cambridge Crystallographic Data Centre (CCDC 1908277).

2.5 | Chromatography

HPLC grade ethanol (EtOH), 2-propanol (2-PrOH), MeOH, CH_3CN, and *n*-hexane (Hex) were purchased from Sigma-Aldrich Co (St Louis, Missouri). Ultrapure water was produced by a Millipore Milli-Q system (Millipore, Bedford, Massachusetts). Commercial chiral analytes used to evaluate the CSPs, trifluoroacetic acid

(TFA), and TEA were obtained from Sigma-Aldrich (St Louis, Missouri) or Merck (Darmstadt, Germany). The "in-house" chiral analytes were synthesized previously by our group.[35,36] Working solutions of all chiral analytes were prepared using HPLC grade EtOH at a concentration of 10 μg mL^{-1}, and the injection volume was 10 μL. The HPLC system comprised a Jasco model 880-PU Intelligent HPLC pump (JASCO Corporation, Tokyo, Japan), equipped with a 7125 injector (Rheodyne LCC, Rohnert Park, California) fitted with a 20-μL loop, a JASCO model 880-30 solvent mixer involving an 875-UV intelligent UV-vis detector. The data were handled on ChromNAC Chromatography Data System (version 1.19.1) from JASCO Corporation (Tokyo, Japan). The mobile phases were prepared in a volume/volume ratio and degassed in an ultrasonic bath for 15 minutes before use. The chromatographic analyses were carried out in isocratic mode at 22 ± 2°C, in triplicate, at a flow rate of 0.2 mL min^{-1}. The UV detection was performed at a wavelength of 254 nm. The column void time was considered to be equal to the peak of the solvent front and was taken from each particular run.

2.6 | Computational

The structures of the synthesized selectors were drawn in Chemdraw and minimized in Chem3D 16.0, and both enantiomers of analytes were drawn and minimized using an Austin Model 1 (AM1) semi-empirical quantum mechanics force field.[37] The calculation was finished when the gradient between any two successive steps in the geometry search was less than 10^{-1} kcal mol^{-1} $Å^{-2}$ or the maximum steps were reached, whichever comes first. The line search used was the Broyden-Fletcher-Golfarb-Shanno search, which uses an approximate Hessian matrix to guide the search.[38] Docking simulations between the synthesized chiral selectors and the analytes were undertaken in AutoDock Vina (Molecular Graphics Lab, La Jolla, California).[39] AutoDock Vina considered the target conformation as a rigid unit while the ligands were allowed to be flexible and adaptable to the target. Vina searched for the lowest binding affinity conformations and returned nine different conformations for each small molecule. The lowest binding energy docking poses of each compound were chosen. AutoDock Vina was run using an exhaustiveness of 8, and grid boxes with dimensions 16.0, 15.0, and 13.0 engulfing the selectors were built. PyMol v1.3 (Schrödinger, New York, New York)[40] was used to visualize the conformations and interactions as well as the graphical representations.

3 | RESULTS AND DISCUSSION

Our previous results of enantioselectivity obtained with recent CSPs based on CDXs,[14] the structural attributes of those small molecules for suitability as chiral selectors, and the high enantioselectivity observed for a series of CDXs in diverse CSPs[2,3,23-25] were crucial to pursue this approach and explore other strategies with CDXs as chiral selectors. Therefore, we report herein the preparation and evaluation of the LC enantioresolution behavior of twelve new CSPs (CSPs **1-12**) (Figures 1 and 2).

The synthetic routes for preparation of the new CSPs are shown in Schemes S1 to S4. Nine different hydroxylated small molecules (**1-9**) were selected as a basis for molecular modifications. The hydroxy-9*H*-xanthen-9-ones **1-5** were obtained through the condensation of appropriate building blocks in the presence of Lewis acid $ZnCl_2$ (**1**)[31] or P_2O_5/$MeSO_3H$ (Eaton's reagent) (**2-5**)[27-29,32] (Scheme S1). A dehydrative cyclization of 2,2′,4,4′-tetrahydroxybenzophenone (**9**) in a furnace at 200°C afforded the 3,6-dihydroxy-9*H*-xanthen-9-one (**6**),[30] in a very high yield (99%) (Scheme S2). The 3,4-dihydroxy-9*H*-xanthen-9-one (**7**) was synthetized by a classical intramolecular acylation of a benzophenone intermediate and further demethylation[31] (Scheme S3). The commercially available 2,2′,4,4′-tetrahydroxybenzophenone (**9**) and 4,4′-dihydroxybenzophenone (**8**) were also used as building blocks for preparation of new CSPs (Scheme S4). The hydroxylated small molecules (**1-9**) were further oxidized to afford acetate intermediates (**10-18**) and then carboxylated derivatives (**19-27**). The synthetic procedure to obtain the acetate intermediates (**10-18**) involved a Williamson ether synthesis using an alkyl halide containing an ester group ($BrCH_2COOCH_3$). Then, resorting to an alkaline hydrolysis of the respective esters, the carboxylated derivatives (**19-27**) were obtained. Compounds comprising a carboxylic acid, such as carboxyxanthones, have already proved to be suitable molecular scaffolds for synthesis of analogues and derivatives, including chiral compounds.[41] The chiral selectors (**28-39**) were synthetized by coupling the carboxylated derivatives (**19-27**) with commercially available enantiomerically pure amino alcohols at room temperature. The synthetic strategy was based on previous works using TBTU as a coupling reagent, in the presence of a catalytic amount of TEA in THF as solvent,[35,36] providing good yields. The structures of the chiral selectors **28-39** and all intermediates were successfully established, and for hydroxy-9*H*-xanthen-9-ones (**1-7**), all the data were in accordance with the literature.[28,30,42-45] The enantiomeric ratio (e.r.) of all chiral selectors was determined by LC[46] using two commercial chiral columns, (*S*,*S*)-Whelk-O1 and Lux Celullose-2, and was higher than 99%. The next step

was the synthesis of silylated derivatives, by reaction with 3-(triethoxysilyl)propylisocyanate,[47,48] to allow the further covalent linkage of the chiral selectors to a chromatographic support (silica gel, Nucleosil-100-5), affording CSPs **1-12** (Figures 1 and 2). Therefore, after the synthesis of suitable chemical substrates, the carboxylated derivatives **19-27**, all CSPs were prepared through simple three steps: amidation, silylation, and bonding to silica gel.

The majority of the new CSPs was covalently bonded to silica gel within appropriate levels (0.61-2.32 μmol m^{-2} based on carbon), as shown in Table 1, when compared with previous CSPs.[14] It was found that for some CSPs (**1**, **5-8**) the percent of selector loading based on nitrogen analysis was higher than the percent based on carbon. This may be because often the ethoxy groups of the siloxanes are not fully hydrolyzed. The silica gels in CSPs **9** and **12** contain about 0.30 μmol m^{-2}. It is assumed that the lower amount of loaded chiral selectors in those CSPs was caused by the low solubility of their silylated chiral selectors in toluene. Even though we conducted additional experiments by testing other solvents such as THF, CH_3CN, and DMSO, the solubility remained low. The columns capacity for enantioresolution is highly dependent on coverage density of CSP; thus, the low chiral selector loading for CSPs **9** and **12** will certainly influence their chromatographic performance.

All the CSPs were packed in LC columns with 150 × 2.1 mm I.D. This internal diameter was chosen because, previously, we demonstrated that columns containing the same chiral selector based on a CDX and only differing in the internal diameters, specifically 4.6 and 2.1 mm, showed similar enantiomeric performance.[14] In fact, by reducing the internal diameter of the LC columns, two main advantages can be pointed out such as a significant reduction of the material to be synthetized and packed and a considerable decrease of the solvent consumption during the packing and chromatographic analysis. The ecological, practical, and economic benefits are undeniable.[49,50]

Initially, several commercial and "in house" chiral analytes (A1-A38) were selected (Figure S1) to evaluate the LC enantioselective performance of CSPs **1-12**. Additionally, enantiomeric mixtures of the chiral selectors (**28-39**) used for its preparation were included. The chromatographic analyses were performed under elution in the normal phase mode, using different proportions of Hex and EtOH or 2-PrOH as mobile phases. Baseline enantioseparation was only obtained for analytes A24 and A30. For the other tested analytes, short retention factors (analysis time generally lower than 3 min) and the absence or poor resolutions were found for all the combinations of mobile phases evaluated. Table 2 shows the overall best results. For the enantioseparated analytes, the elution order was determined by injecting each enantiomer separately.

Taking into account that in our previous work, the best enantioselectivity was achieved with two xanthone-(*R*)-(−)-α-phenylglycinol-derived CSPs,[14] we first developed the CSP **1** comprising a chiral selector based on a xanthone derivative with a chiral moiety derived from (*R*)-(−)-α-phenylglycinol (**52**) in position 1 of the xanthone scaffold (**28**) (Figure 1). The strategy was to use the same chiral moiety but changing its position in the xanthone scaffold. It was found that CSP **1** showed good enantioselectivity, α values of 2.02 and 2.04, and resolution, R_s values of 2.44 and 2.13, for A24 and A30, respectively, using Hex: EtOH (90:10 *v*/*v*) as mobile phase. Moreover, in this mobile phase, the theoretical plate numbers (*N*) for the first and second eluted enantiomers were 242/349 and 206/509 for A24 and A30, respectively.

The next step was the introduction of an extra chiral moiety affording CSP **2** (Figure 1). The aim was to attempt more versatility and better enantioresolution by increasing the number of chiral moieties for enantiorecognition. Nevertheless, CSP **2** comprising two chiral moieties in positions 3 and 6 of the xanthone scaffold (symmetrical structure) presented similar chromatographic performance to CSP **1**, showing only a slight increase of retention as well as enantioselectivity and resolution for A24 and A30 (Table 2). Nevertheless, an increasing of the efficiency was observed, being the *N* values for the first and second eluted enantiomers of A24 and A30 744/832 and 636/788, respectively, in Hex: EtOH (80:20 *v*/*v*).

For comparison purposes, in addition to the (*R*)-(−)-α-phenylglycinol (**52**), the amino alcohols (*S*)-(+)-leucinol (**53**) and (*S*)-(+)-valinol (**54**) were chosen to obtain CSPs **3** and **4**, respectively (Figure 1). Surprisingly, both CSPs showed similar enantioselectivity and resolution to those of CSP **2** for the enantioseparated analytes (A24 and A30), as shown in Table 2. For CSP **3**, the *N* values for the first and second eluted enantiomers were 371/295 and 266/270 for A24 and A30, respectively, using Hex: EtOH (80:20 *v*/*v*) as mobile phase; while for CSP **4,** the *N* values were 291/344 and 528/655.

An advantage of CSPs comprising small molecules as selectors is the possibility of inversion of elution order by preparation of two different CSPs switching the configuration of the chiral selector.[11] Previously, we have confirmed the inversion of elution order for a selector based on a xanthone derivative comprising one chiral aromatic moiety.[14] To verify if with selectors comprising two chiral aromatic moieties the inversion of elution order would occur, CSP **5** was prepared. The selector of this CSP is

TABLE 2 Chromatographic enantioseparation of analytes A24 and A30 on CSPs **1-12**

		A24			A30		
	Mobile Phase (*v*/*v*)	k_1	α	R_s	k_1	α	R_s
CSP **1**	Hex/EtOH: 90/10	1.50	2.02	2.44	1.84	2.04	2.13
	Hex/EtOH: 80/20	0.61	1.69	1.15	0.93	1.73	1.21
	Hex/2-PrOH: 80/20	0.64	2.26	1.66	0.79	2.21	1.52
CSP **2**	Hex/EtOH: 80/20	2.40	1.92	3.50	2.39	2.13	3.81
	Hex/EtOH: 70/30	1.63	1.74	2.61	1.53	2.03	3.11
	Hex/2-PrOH: 80/20	3.22	2.51	3.38	3.00	3.02	3.71
	Hex/2-PrOH: 70/30	2.03	2.19	2.56	1.75	2.83	3.13
CSP **3**	Hex/EtOH: 90/10	2.36	2.00	1.95	3.26	1.74	1.67
	Hex/EtOH: 80/20	1.58	1.86	1.88	1.83	1.63	1.36
	Hex/EtOH: 70/30	0.99	1.59	<1.00	0.99	1.62	1.06
	Hex/2-PrOH: 80/20	1.91	2.31	2.26	2.05	1.93	1.83
	Hex/2-PrOH: 70/30	1.36	1.49	1.15	1.21	1.87	1.29
CSP **4**	Hex/EtOH: 90/10	2.24	2.16	3.20	2.59	2.22	3.73
	Hex/EtOH: 80/20	1.02	1.89	1.66	1.68	2.09	2.12
	Hex/EtOH: 70/30	0.86	1.46	1.17	0.71	1.93	2.08
	Hex/2-PrOH: 80/20	0.95	2.00	1.95	1.16	1.91	1.70
	Hex/2-PrOH: 70/30	0.61	1.80	1.46	0.91	1.52	1.00
CSP **5**	Hex/EtOH: 80/20	2.09	2.29	1.33	1.75	3.33	1.74
	Hex/EtOH: 70/30	1.44	2.16	1.11	1.06	3.48	1.64
	Hex/2-PrOH: 80/20	1.82	2.29	1.09	3.28	2.24	1.76
	Hex/2-PrOH: 70/30	1.73	2.08	1.08	1.10	3.01	1.59
CSP **6**	Hex/EtOH: 90/10	0.55	2.25	<1.00	0.99	1.00	ND
	Hex/EtOH: 80/20	0.34	1.27	<1.00	0.39	1.00	ND
	Hex/2-PrOH: 80/20	0.22	2.48	<1.00	0.26	1.00	ND
CSP **7**	Hex/EtOH: 80/20	2.13	1.61	1.61	2.08	2.37	2.91
	Hex/2-PrOH: 80/20	2.01	1.81	1.48	1.65	2.98	2.54
CSP **8**	Hex/EtOH: 90/10	2.63	2.43	<1.00	2.96	2.57	<1.00
	Hex/EtOH: 80/20	1.43	2.05	<1.00	1.46	1.00	<1.00
CSP **9**	Hex/EtOH: 90/10	1.62	2.28	1.68	2.25	1.00	ND
	Hex/EtOH: 80/20	0.75	1.86	1.32	0.96	1.00	ND
	Hex/EtOH: 70/30	0.32	1.56	<1.00	0.38	1.00	ND
CSP **10**	Hex/EtOH: 90/10	2.55	2.41	2.02	3.15	2.05	1.59
	Hex/EtOH: 80/20	1.43	2.02	1.36	1.29	2.12	1.22
	Hex/2-PrOH: 80/20	1.10	2.30	1.31	1.08	2.55	1.56
CSP **11**	Hex/EtOH: 90/10	1.68	2.07	2.15	1.68	2.13	2.24
	Hex/EtOH: 80/20	1.14	1.84	1.56	0.99	2.17	1.88
	Hex/EtOH: 70/30	0.69	1.67	<1.00	0.59	1.98	1.24
	Hex/2-PrOH: 80/20	1.21	2.57	1.69	0.78	2.28	1.27
	Hex/2-PrOH: 70/30	0.75	1.77	1.11	0.55	1.25	1.38
CSP **12**	Hex/EtOH: 90/10	3.00	2.20	3.56	3.70	1.96	3.04
	Hex/EtOH: 80/20	1.32	1.87	2.24	1.41	1.68	1.69
	Hex/EtOH: 70/30	0.70	1.71	1.30	0.70	1.56	1.15
	Hex/2-PrOH: 80/20	1.17	2.07	1.57	1.16	2.00	1.95
	Hex/2-PrOH: 70/30	1.02	2.13	1.75	0.89	2.09	1.72

Note. ND, not determined. Detection at 254 nm; flow rate, 0.2 mL min^{-1}. Size of all columns: 150 mm length, 2.1 mm I.D.

the enantiomeric pair of CSP **2** selector. In this study, with more structurally complex xanthone selectors, it was found that the inversion of elution order did not occur for the enantioseparated analytes (A24 and A30). The results obtained in the subsequent docking studies justify why.

Two more CSPs comprising two chiral moieties derived from (*R*)-(−)-α-phenylglycinol in different

positions in the xanthone scaffold, specifically positions 1 and 3 (CSP **6**) and positions 3 and 4 (CSP **7**) (Figure 1) were developed. It was found that CSP **7** enantioseparated the same two analytes with equivalent enantioselectivity and resolution, compared with CSP **2**. As example, for analyte A30, using Hex:EtOH (80:20 *v*/*v*) as a mobile phase, the α and R_s values obtained on CSP **2** were 2.13 and 3.81, while for CSP **7**, those values were 2.37 and 2.91, respectively. However, CSP **7** showed lower efficiency, being the *N* values for the first and second eluted enantiomers of A24 and A30 360/349 and 334/337, respectively, in Hex: EtOH (80:20 *v*/*v*). CSP **6** showed some enantioselectivity only for analyte A24, however, with poor resolution ($R_s < 1.00$ in all tested mobile phases).

The next step was to work with an increase of the number of chiral moieties to three (CSPs **8** and **9**) and four (CSP **10**) (Figure 1). It was found that both CSPs comprising three chiral moieties presented less discrimination ability. Nevertheless, CSP **10** comprising chiral units in positions 1, 3, 6, and 8 of xanthone scaffold (symmetrical structure) showed good chromatographic results for both analytes A24 and A30, as shown in Table 2.

In order to understand the role of the rigidity of the *quasi*-planar structure of the xanthone scaffold in the enantioresolution properties of these CSPs and also aiming to improve the enantioselectivity by increasing the flexibility of the central aromatic core, CSPs **11** and **12** were prepared (Figure 2). These CSPs are derived from benzophenone derivatives, one of the most common intermediates for the synthesis of xanthones.[51,52] It was found that CSPs **11** and **12** afforded similar chromatographic results to their xanthone-based analogue CSPs, specifically CSPs **5** and **10** (Table 2).

Regarding the influence of the organic modifier in the mobile phase, it was found that, despite a slight increase of enantioselectivity observed for Hex/2-PrOH combinations, shorter retention factors and higher resolution were obtained using mixtures of Hex and EtOH. For these reasons, the use of EtOH was a better choice. Regarding the elution order, for the enantioseparated analytes, the (*R*)-enantiomer was the more retained in all CSPs. In Figures 3 and 4, a set of selected

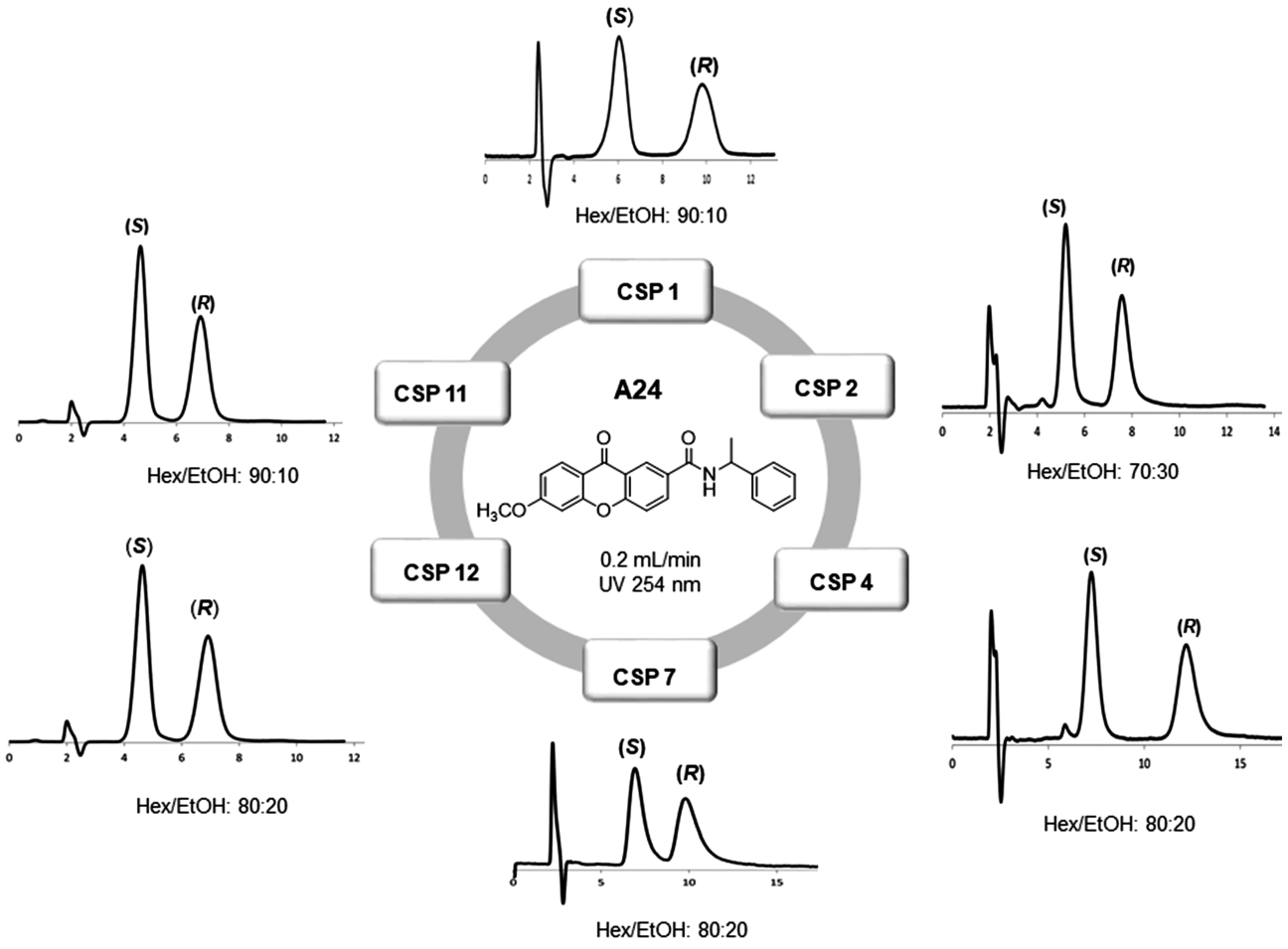

FIGURE 3 Chromatograms for the enantioseparation of analyte A24 on different CSPs, at optimized chromatographic conditions

chromatograms for analytes A24 and A30 in different CSPs are presented.

In order to understand the binding mechanism behind the observed results of enantioresolution, docking studies were performed using the selectors of CSPs **1-12**. The structure of the chiral selector of CSP **1** (compound **28**) was determined by single crystal X-Ray diffraction, and its ortep view is shown in Figure 5.

The central pyranoid ring has a partial aromatic character, and as usual, the xanthone skeleton adopts a kind of flattened boat conformation.[53] The absolute configuration of the chiral center of the compound was confirmed to be (*R*) by X-Ray analysis.

Values of docking scores are presented on Table 3. The lower the docking score, the more stable the analyte-selector complex is. Docking scores between −3.4 and − 6.5 kcal mol^{-1} and energy differences from −0.1 to −0.9 $kcalmol^{-1}$ were obtained for A24; and docking scores between −4.0 and − 6.1 kcal mol^{-1} and energy differences from 0 to −0.4 kcal mol^{-1} were obtained for A30.

The binding energies were different for the enantiomers of A24 in CSPs **1-12** and A30 in CSPs **1-5**, **7**, **8**, and **10-12**, indicating that they have different affinities for these selectors, which is in accordance with the chromatographic data (separations were achieved, $\alpha = 1.25$ to 3.02). In contrast, the binding energies were equal for

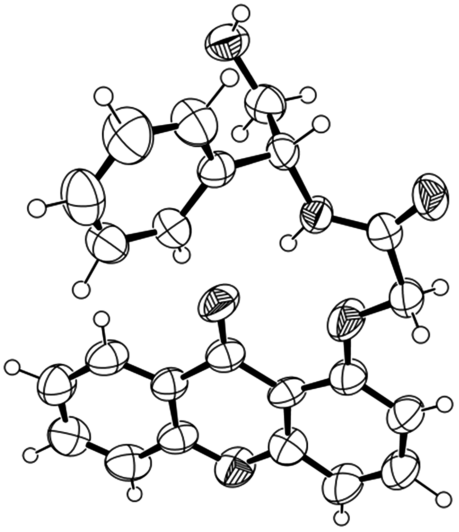

FIGURE 5 Ortep view of the crystal structure of chiral selector **28**

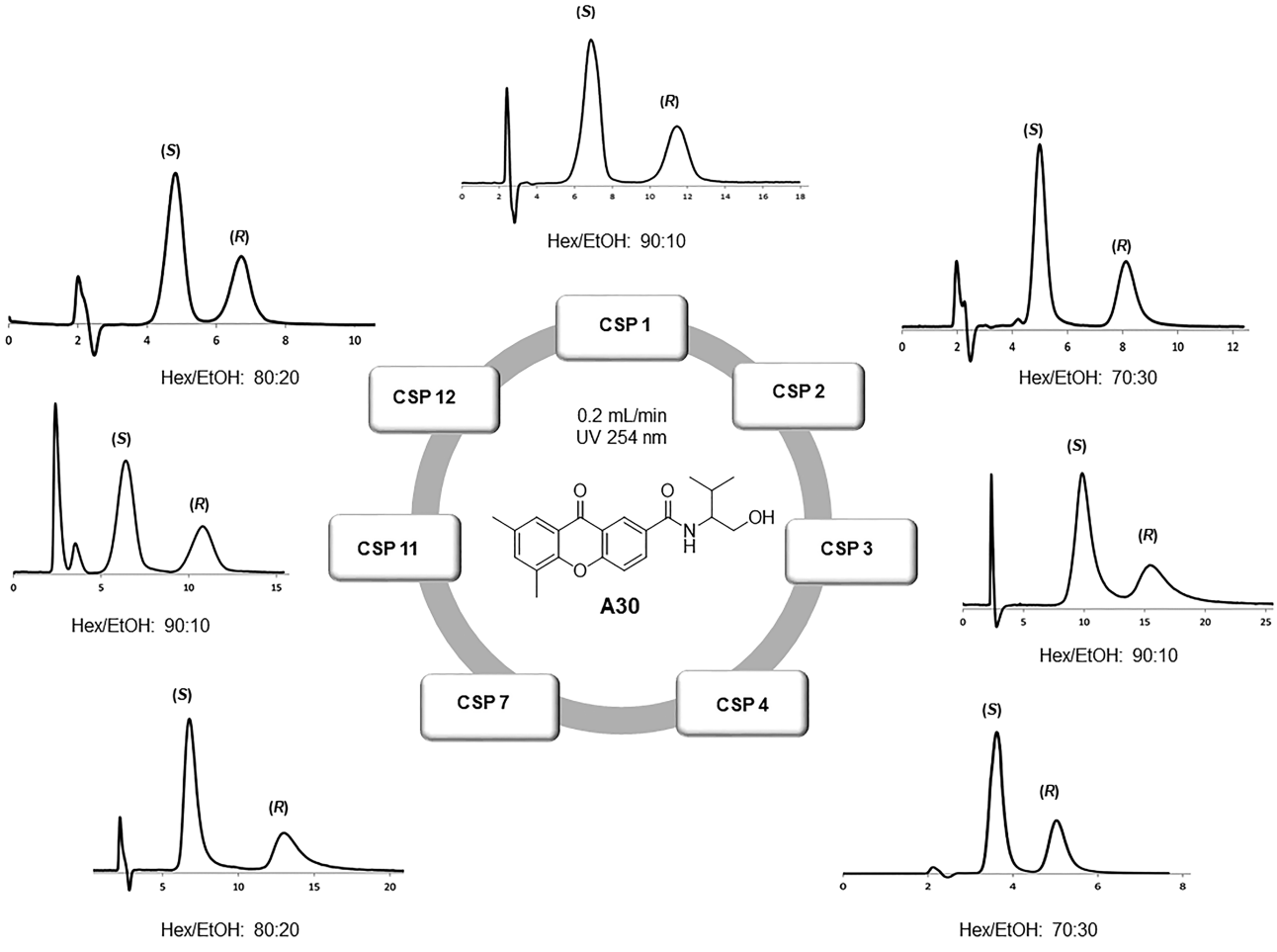

FIGURE 4 Chromatograms for the enantioseparation of analyte A30 on different CSPs, in optimized chromatographic conditions

TABLE 3 Docking scores and elution order of both enantiomers of analytes A24 and A30 on CSPs **1-12**

	A24		A30	
	Docking Score, kcal mol^{-1}	**Energy Difference, kcal mol^{-1}**	**Docking Score, kcal mol^{-1}**	**Energy Difference, kcal mol^{-1}**
CSP **1** (X-ray structure)	(*S*): −4.5 (*R*): −4.8	−0.3	(*S*): −4.5 (*R*): −4.7	−0.2
CSP **2**	(*S*): −5.4 (*R*): −5.5	−0.1	(*S*): −5.2 (*R*): −5.4	−0.2
CSP **3**	(*S*): −5.0 (*R*): −5.1	−0.1	(*S*): −4.6 (*R*): −4.9	−0.3
CSP **4**	(*S*): −5.5 (*R*): −5.7	−0.2	(*S*): −5.1 (*R*): −5.4	−0.3
CSP **5**	(*S*): −5.1 (*R*): −5.6	−0.5	(*S*): −5.0 (*R*): −5.3	−0.2
CSP **6**	(*S*): −5.5 (*R*): −5.7	−0.2	(*S*): −5.2 (*R*): −5.2	0.0
CSP **7**	(*S*): −3.4 (*R*): −3.5	−0.1	(*S*): −4.0 (*R*): −4.4	−0.4
CSP **8**	(*S*): −5.0 (*R*): −5.9	−0.9	(*S*): −4.1 (*R*): −4.2	−0.1
CSP **9**	(*S*): −6.3 (*R*): −6.5	−0.2	(*S*): −6.1 (*R*): −6.1	0.0
CSP **10**	(*S*): −6.0 (*R*): −6.1	−0.1	(*S*): −5.6 (*R*): −5.7	−0.1
CSP **11**	(*S*): −5.3 (*R*): −5.4	−0.1	(*S*): −5.0 (*R*): −5.2	−0.2
CSP **12**	(*S*): −6.0 (*R*): −6.1	−0.1	(*S*): −5.6 (*R*): −5.7	−0.1

both enantiomers of A30 in CSP **6** (−5.2 kcal mol^{-1}) and CSP **9** (−6.1 kcal mol^{-1}), indicating that they have identical affinity for these selectors, which is in agreement with the experimental results (no separation was achieved, $\alpha = 1.00$). Docking analytes into selectors of CSPs **1-12** revealed that the (*R*)-enantiomers had higher affinity to the target (lower docking scores) than the corresponding (*S*)-enantiomers, although the average docking score difference was small in some cases. Consequently, there was 100% agreement between docking scores and experimental results for enantioselectivity and elution order of the enantiomers of the chiral analytes in all CSPs.

In order to understand the binding mechanism and the chromatographic results, a visual inspection of the binding conformations and established interactions were performed.

Figure 6A illustrates a representative example of the most stable docked conformations for enantiomers of

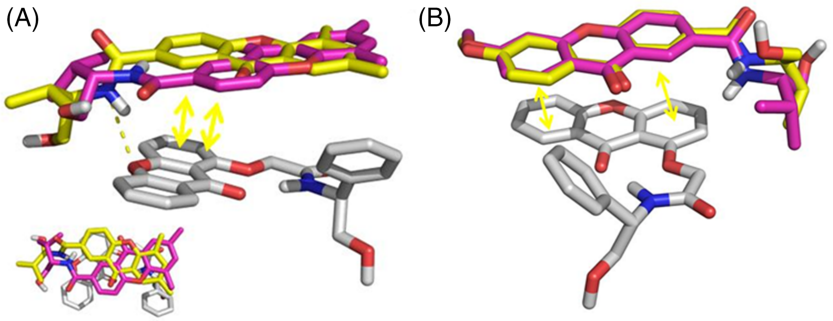

FIGURE 6 (A) Crystallographic selector of CSP **1** and docked A30 enantiomers (top-view of the docking poses is represented on the bottom-left corner of the image); (B) A17 docking pose of A17 enantiomers on crystallographic selector of CSP **1**. Selector of CSP **1** is represented as grey sticks; (*R*) and (*S*) enantiomers are represented as yellow and pink sticks, respectively. Hydrogen interactions and π-stacking interactions are represented in yellow broken lines and yellow double arrow, respectively

analyte A30 complexed with the chiral selector of CSP **1**. The (*R*)-enantiomer of A30 was more retained in the CSP and, accordingly, presented lower docking score than the (*S*)-enantiomer. In fact, only the (*R*)-enantiomer binds in a conformation that allows the establishment of a hydrogen interaction with the ether group of the xanthone tricyclic system of the selector. Furthermore, the tricyclic ring system of (*R*)-enantiomer establishes parallel π-stacking interactions with the xanthone scaffold of the selector, while its antipoda establishes parallel-displaced π-stacking interactions (Figure 6A). On the other hand, regarding for example analyte A17, which have the same chiral moiety as analyte A30 only differing in the nature, number, and positions of the substituents on the xanthone scaffold (Figure S1), both enantiomers docked on the identical docking pose with the tricyclic ring systems superimposed and an RMSD of only 1.5 Å (Figure 6B). It was found that A17 enantiomers, which were not separated on CSP **1**, only established π-stacking interactions with the selector of CSP **1**.

It is also important to highlight that, through docking studies, it was confirmed that the aromatic ring bonded to the stereogenic center of the side chain of the selector is not involved in interactions with analytes, as shown in Figure 7A,B. The same occurs when the group is an alkyl chain. This justifies the reason why CSPs **2** and **5** (derived from phenylglycinol), CSP **3** (derived from leucinol), and CSP **4** (derived from valinol) have similar chromatographic behavior. It was found that with selectors of CSPs comprising three chiral units (CSPs **8** and **9**), the interactions responsible for the enantioselectivity did not occur successfully due to steric hindrance of the three bulky chiral moieties preventing the establishment of parallel π-stacking interactions between the xanthone scaffolds of analytes and selectors. Moreover, the available space for the interactions between these two CSPs and the enantiomers is smaller. For selectors of CSPs comprising four bulky chiral moieties (CSPs **10** and **12**), they are in positions of the xanthone or benzophenone scaffold allowing to establish the interactions essential for enantiomeric discrimination (Figure 7C,D). Regarding CSP **10**, for example, enantiomers of A30 docks on the same side of the selector, but with the carbonyl group of the xanthone scaffold pointing in opposite directions. Therefore, the (*R*)-enantiomer is able to form two hydrogen interactions through the xanthone carbonyl and side chain hydroxyl groups. The (*S*)-enantiomer establishes only one hydrogen interaction (Figure 7C). As far as CSP **12** is concerned, the enantiomers of A30 also dock on the same side of the selector. The (*S*)-enantiomer of A30 establishes three hydrogen interactions with the benzophenone carbonyl group, amide, and hydroxyl groups of the side chains of the selector. The (*R*)-enantiomer of A30 only establishes one hydrogen interaction by means of the side chain hydroxyl group, but it establishes additional π-stacking interactions (parallel and T-shaped) (Figure 7D).

Regardless the nature of the central aromatic core of the selector, xanthone for CSP **10** or benzophenone for CSP **12**, both CSPs were able to establish parallel π-stacking interactions with (*R*)-enantiomer of analyte A30 that, in addition to other interactions, are

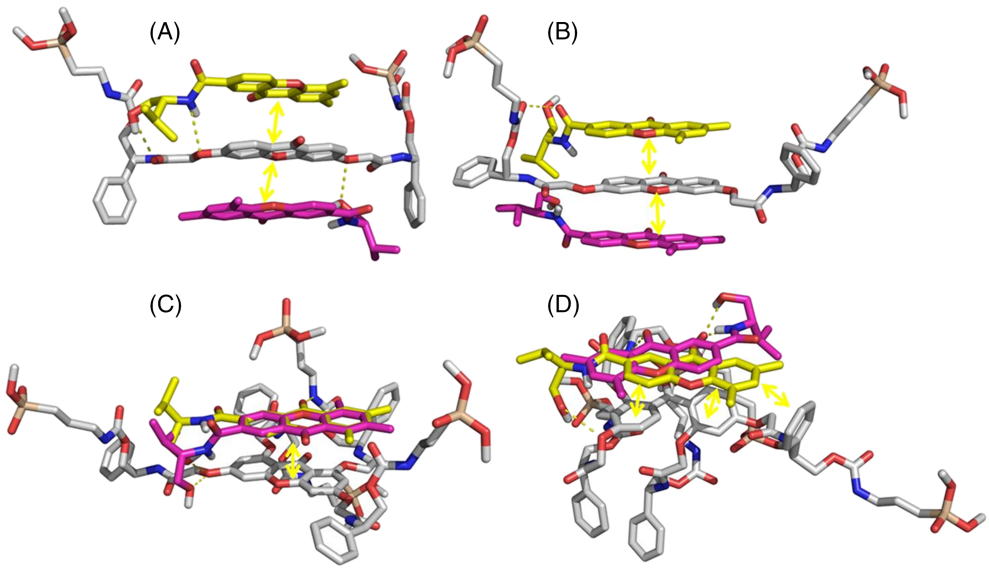

FIGURE 7 (A) Selector of CSP **2** and docked A30 enantiomers; (B) selector of CSP **5** and docked A30 enantiomers; (C) selector of CSP **10** and docked A30 enantiomers; (D) selector of CSP **12** and docked A30 enantiomers. Selectors of CSPs **2**, **5**, **10**, and **12** are represented as grey sticks; (*R*) and (*S*) enantiomers are represented as yellow and pink sticks, respectively. Hydrogen interactions and π-stacking interactions are represented in yellow broken lines and yellow double arrow, respectively

responsible for enantioselectivity that explains the similar enantioresolution properties of these CSPs.

To enlarge the number of enantiomeric separations, 24 more chiral analytes were selected, including structurally diverse commercial compounds from different chemical nature (neutral, acid, and basic). Moreover, the chromatographic analysis was performed using several mobile phases in the three elution modes (normal phase, polar organic, and reversed-phase elution conditions) for all the tested analytes (including the enantiomeric mixtures of the chiral selectors (**28-39**) and analytes A1-A38. Considering that the majority of the new CSPs presented similar enantioselective performance, as they enantioseparated the same two analytes (A24 and A30), CSP **2** was selected to carried out further analysis since it showed the best efficiency in the previous chromatographic evaluation. The overall best results were summarized in Table 4.

Excellent enantioselectivity, α value of 5.08, and resolution, R_s value of 3.13, were obtained for 4-methoxy-α-methylbenzylamine, in reversed-phase mode, using CH_3CN/H_2O/TEA: 80/20/0.01 as mobile phase. Moreover, enantioselectivity was also obtained for other analytes, including the commercial amines *N*-benzyl-1-(1-naphthyl)ethylamine and alanine-2-naphthylamide, although with low resolution (Table 4). Therefore, the chromatographic performance of the new CSPs for enantioseparation of a large library of chiral amines should be further investigated.

TABLE 4 Chromatographic data obtained on CSP **2** (not include analytes A24 and A30)

Analyte	Mobile Phase (*v*/*v*)	k_1	α	R_s
4-Methoxy-α-methylbenzylamine	CH_3CN/H_2O/TEA: 80/20/0.01	0.23	5.08	3.13
N-Benzyl-1-(1-naphthyl)ethylamine	CH_3CN/H_2O/TEA: 80/20/0.01	0.82	1.44	<1.00
Alanine-2-naphthylamide	Hex/EtOH/TEA: 90/10/0.01	3.28	1.36	<1.00
Enantiomeric mixture of 28	CH_3CN: 100	0.95	1.42	<1.00
Enantiomeric mixture of 35	CH_3CN/MeOH: 80/20	0.40	1.33	<1.00
A5[a]	Hex/EtOH: 80/20	3.40	1.28	1.00
A17[a]	CH_3CN: 100	1.38	1.78	<1.00
A19[a]	CH_3CN/MeOH: 80/20	0.41	1.17	<1.00
A20[a]	CH_3CN/MeOH: 80/20	0.42	1.10	<1.00
A27[a]	CH_3CN/EtOH: 80/20	0.38	1.39	<1.00
A28[a]	CH_3CN/EtOH: 80/20	0.37	1.39	<1.00

Note. Detection at 254 nm; flow rate, 0.2 mL min^{-1}.

[a]Chemical structures shown in Figure S1.

4 | CONCLUSION

Twelve new CSPs were successfully prepared aiming to obtain versatile and efficient CSPs as well as to explore the role of some structural characteristics that could be crucial for enantiorecognition. It was found that the number and position of the chiral units positioned in the xanthone scaffold of the chiral selectors can interfere with the chiral recognition mechanism by steric hindrance. Moreover, for the CSPs comprising equal numbers of chiral units in the same positions, the nature of the substituent next to the stereogenic center was shown not to be pivotal because either the CSPs having an aromatic ring or an alkyl chain showed similar results. The central aromatic core of the selector, either xanthone or benzophenone scaffold, aligned with the xanthone tricyclic ring of the analytes to maximize π-stacking interactions, and the hydrogen bonding interactions between the donor and acceptor polar groups of analytes and selectors, demonstrated to be essential for enantioselective recognition. The docking studies proved to be a meaningful tool for the structural requirements necessary for the effective elucidation of the intermolecular CSP-analyte interactions.

The development of new CSPs for LC is a continuous and challenging issue. This work is an important contribution to improve the design of new selectors and further preparation of more efficient CSPs based on xanthone and benzophenone derivatives possessing wider applicability.

ACKNOWLEDGMENTS

This work was supported by the Strategic Funding UID/Multi/04423/2019 through national funds provided by FCT—Foundation for Science and Technology and European Regional Development Fund (ERDF), through the COMPETE – Programa Operacional Factores de Competitividade (POFC) program in the framework of the program PT2020; the project PTDC/MAR-BIO/4694/2014 (reference POCI-01-0145-FEDER-016790 and 3599-PPCDT), co-financed by COMPETE 2020, under the PORTUGAL 2020 Partnership Agreement, through the European Regional Development Fund (ERDF), CHIRALBIOACTIVE-PI-3RL-IINFACTS-2019 financed by IINFACTS and QOPNA research project (FCT UID/QUI/00062/2019), and Portuguese NMR

network. Y.Z. Phyo thanks the Erasmus Mundus Action 2 (Lotus Plus project) for a PhD scholarship.

ORCID

Maria Elizabeth Tiritan https://orcid.org/0000-0003-3320-730X
Carla Fernandes https://orcid.org/0000-0003-0940-9163

REFERENCES AND NOTES

1. Gumustas M, Ozkan SA, Chankvetadze B. Analytical and preparative scale separation of enantiomers of chiral drugs by chromatography and related methods. *Curr Med Chem*. 2018;25(33):4152-4188.
2. Fernandes C, Brandão P, Santos A, et al. Resolution and determination of enantiomeric purity of new chiral derivatives of xanthones using polysaccharide-based stationary phases. *J Chromatogr a*. 2012;1269:143-153.
3. Fernandes C, Palmeira A, Santos A, Tiritan ME, Afonso C, Pinto MM. Enantioresolution of chiral derivatives of xanthones on (*S*,*S*)-Whelk-O1 and L-phenylglycine stationary phases and chiral recognition mechanism by docking approach for (*S*,*S*)-Whelk-O1. *Chirality*. 2013;25(2):89-100.
4. Silva C, Ribeiro C, Maia AS, Gonçalves V, Tiritan ME, Afonso C. Enantiomeric separation of tramadol and its metabolites: method validation and application to environmental samples. *Symmetry*. 2017;9(9).
5. Silva B, Fernandes C, Tiritan ME, et al. Chiral enantioresolution of cathinone derivatives present in "legal highs", and enantioselectivity evaluation on cytotoxicity of 3,4-methylenedioxypyrovalerone (MDPV). *Forensic Toxicol*. 2016;1-14.
6. Sousa ME, Tiritan ME, Belaz KRA, et al. Multimilligram enantioresolution of low-solubility xanthonolignoids on polysaccharide chiral stationary phases using a solid-phase injection system. *J Chromatogr a*. 2006;1120(1–2):75-81.
7. Silva B, Pereira JA, Cravo S, et al. Multi-milligram resolution and determination of absolute configuration of pentedrone and methylone enantiomers. *J Chromatogr B Analyt Technol Biomed Life Sci*. 2018;1100–1101:158-164.
8. Ribeiro J, Tiritan ME, Pinto MMM, Fernandes C. Chiral stationary phases for liquid chromatography based on chitin- and chitosan-derived marine polysaccharides. *Symmetry*. 2017;9(9):1-28.
9. Tang M, Zhang J, Zhuang S, Liu W. Development of chiral stationary phases for high-performance liquid chromatographic separation. *TrAC - Trends Anal Chem*. 2012;39:180-194.
10. Felix G, Berthod A. Commercial chiral stationary phases for the separations of clinical racemic drugs. *Sep Purif Rev*. 2007;36(4):285-481.
11. Teixeira J, Tiritan ME, Pinto MMM, Fernandes C. Chiral stationary phases for liquid chromatography: recent developments. *Molecules*. 2019;24:865. https://doi.org/10.3390/molecules24050865
12. Fernandes C, Phyo YZ, Silva AS, Tiritan ME, Kijjoa A, Pinto MMM. Chiral stationary phases based on small molecules: an update of the last 17 years. *Sep Pur Rev*. 2018;47(2):89-123.
13. Fernandes C, Tiritan ME, Pinto M. Small molecules as chromatographic tools for HPLC enantiomeric resolution: Pirkle-type chiral stationary phases evolution. *Chromatographia*. 2013;76(15–16):871-897.
14. Fernandes C, Tiritan ME, Cravo S, et al. New chiral stationary phases based on xanthone derivatives for liquid chromatography. *Chirality*. 2017;29(8):430-442.
15. Araújo J, Fernandes C, Pinto M, Tiritan ME.*Chiral derivatives of xanthones with antimicrobial activity*. Molecules, 2019;24(2). https://doi.org/10.3390/molecules24020314.
16. Fernandes C, Carraro ML, Ribeiro J, Araújo J, Tiritan ME, Pinto MMM. Synthetic chiral derivatives of xanthones: biological activities and enantioselectivity studies. *Molecules*. 2019;24(4):791. https://doi.org/10.3390/molecules24040791
17. Yu J, Armstrong DW, Ryoo JJ. Synthesis of new C3 symmetric amino acid- and aminoalcohol-containing chiral stationary phases and application to HPLC enantioseparations. *Chirality*. 2018;30(1):74-84.
18. Yu J, Lee JM, Ryoo JJ. Chiral separation on various modified amino alcohol-derived HPLC chiral stationary phases. *Chirality*. 2016;28(4):276-281.
19. Yu J, Ryoo DH, Lee JM, Ryoo JJ. Synthesis and application of C2 and C3 symmetric (*R*)-phenylglycinol-derived chiral stationary phases. *Chirality*. 2016;28(3):186-191.
20. Mayani VJ, Abdi SHR, Kureshy RI, Khan NH, Agrawal S, Jasra RV. Synthesis and characterization of (*S*)-amino alcohol modified M41S as effective material for the enantioseparation of racemic compounds. *J Chromatogr a*. 2006;1135(2):186-193.
21. Scriba GKE. Chiral recognition mechanisms in analytical separation sciences. *Chromatographia*. 2012;75(15–16):815-838.
22. Scriba GKE. Chiral recognition in separation science—an update. *J Chromatogr a*. 2016;1467:56-78.
23. Phyo YZ, Cravo S, Palmeira A, et al. Enantiomeric resolution and docking studies of chiral xanthonic derivatives on chirobiotic columns. *Molecules*. 2018;23(1):142. https://doi.org/10.3390/molecules23010142
24. Carraro ML, Palmeira A, Tiritan ME, Fernandes C, Pinto MMM. Resolution, determination of enantiomeric purity and chiral recognition mechanism of new xanthone derivatives on (*S*,*S*)-Whelk-O1 stationary phase. *Chirality* 2017:1–10.
25. Fernandes C, Tiritan ME, Cass Q, Kairys V, Fernandes MX, Pinto M. Enantioseparation and chiral recognition mechanism of new chiral derivatives of xanthones on macrocyclic antibiotic stationary phases. *J Chromatogr a*. 2012;1241:60-68.
26. Blodgett J, Wang Y, Li T, et al. Resolution of *tert*-butyl-1-(2-methylnaphthyl)phosphine oxide using selectors identified from a chemical combinatorial library. *Anal Chem*. 2002;74(20):5212-5216.
27. Chan KL, Lai-Yeng T, Yang ML, Syed AAS, Jean-Frederic FW. Synthesis of 1,3,6-trioxygenated prenylated xanthone derivatives as potential antitumor agents. *Lett Org Chem*. 2012;9(8):549-555.
28. Cruz I, Puthongking P, Cravo S, et al. Xanthone and flavone derivatives as dual agents with acetylcholinesterase inhibition

and antioxidant activity as potential anti-Alzheimer agents. *J Chem*. 2017;2017.

29. Pillai RKM, Naiksatam P, Johnson F, Rajagopalan R, Watts PC, Cricchio R, Borras S. Thermorubin II. 1,3-Dihydroxy-9*H*-xanthones and 1,3-dihydroxy-9*H*-xanthenes. New methods of synthesis. *J Org Chem* 1986;51(5):717–723.
30. Pinto E, Afonso C, Duarte S, et al. Antifungal activity of xanthones: evaluation of their effect on ergosterol biosynthesis by high-performance liquid chromatography. *Chem Biol Drug des*. 2011;77(3):212-222.
31. Sousa E, Paiva A, Nazareth N, et al. Bromoalkoxyxanthones as promising antitumor agents: synthesis, crystal structure and effect on human tumor cell lines. *Eur J Med Chem*. 2009;44 (9):3830-3835.
32. Lin S, Koh JJ, Aung TT, Lim F, Li J, Zou H, Wang L, Lakshminarayanan R, Verma C, Wang Y And others. Symmetrically substituted xanthone amphiphiles combat gram-positive bacterial resistance with enhanced membrane selectivity. *J Med Chem* 2017;60(4):1362–1378.
33. Grover P, Shah G, Shah R. Xanthones. Part IV. A new synthesis of hydroxyxanthones and hydroxybenzophenones. *J Chem Soc (Resumed)*. 1955;3982-3985.
34. Sheldrick GM. A short history of SHELX. *Acta Crystallogr Section A: Foundations of Crystallography*. 2008;64(1):112-122.
35. Fernandes C, Masawang K, Tiritan ME, et al. New chiral derivatives of xanthones: synthesis and investigation of enantioselectivity as inhibitors of growth of human tumor cell lines. *Bioorg Med Chem*. 2014;22(3):1049-1062.
36. Fernandes C, Oliveira L, Tiritan ME, et al. Synthesis of new chiral xanthone derivatives acting as nerve conduction blockers in the rat sciatic nerve. *Eur J Med Chem*. 2012;55:1-11.
37. Dewar MJS, Zoebisch EG, Healy EF, Stewart JJP. Development and use of quantum mechanical molecular models. 76. AM1: a new general purpose quantum mechanical molecular model. *J am Chem Soc*. 1985;107(13):3902-3909.
38. Mirzaei H, Zarbafian S, Villar E, et al. Energy minimization on manifolds for docking flexible molecules. *J Chem Theory Comput*. 2015;11(3):1063-1076.
39. Jaghoori MM, Bleijlevens B, Olabarriaga SD. 1001 ways to run AutoDock Vina for virtual screening. *J Comput Aided Mol des*. 2016;30(3):237-249.
40. Seeliger D, de Groot BL. Ligand docking and binding site analysis with PyMOL and Autodock/Vina. *J J Comput Aided Mol Des*. 2010;24(5):417-422.
41. Ribeiro J, Veloso C, Fernandes C, Tiritan ME, Pinto MMM. Carboxyxanthones: bioactive agents and molecular scaffold for synthesis of analogues and derivatives. *Molecules*. 2019;24(1): 180. https://doi.org/10.3390/molecules24010180
42. Carvalho MJ, Carvalho LM, Ferreira AM, Silva AMS. A new xanthone from *Hedychium gardnerianum*. *Nat Prod Res*. 2003;17(6):445-449.
43. Lin C-N, Chung M-I, Liou S-J, Lee T-H, Wang J-P. Synthesis and anti-inflammatory effects of xanthone derivatives. *J Pharm Pharmacol*. 1996;48(5):532-538.
44. Liu Y, Zou L, Ma L, Chen W-H, Wang B, Xu Z-L. Synthesis and pharmacological activities of xanthone derivatives as α-glucosidase inhibitors. *Bioorg Med Chem*. 2006;14(16):5683-5690.
45. Zhang X-J, Ye S-F, Zhang Y, et al. Microwave-assisted efficient and green synthesis of hydroxyxanthone in water. *Synth Commun*. 2012;42(20):2952-2958.
46. Tiritan ME, Fernandes C, Maia AS, Pinto M, Cass QB. Enantiomeric ratios: why so many notations? *J Chromatogr a*. 2018;1569:1-7.
47. Welch CJ, Perrin SR. Improved chiral stationary phase for ß-blocker enantioseparations. *J Chromatogr a*. 1995;690(2):218-225.
48. Ihara T, Sugimoto Y, Asada M, Nakagama T, Hobo T. Influence of the method of preparation of chiral stationary phases on enantiomer separations in high-performance liquid chromatography. *J Chromatogr a*. 1995;694(1):49-56.
49. Sandra P, Vanhoenacker G, David F, Sandra K, Pereira A. Green chromatography (Part 1): introduction and liquid chromatography. *LC-GC Europe* 2010;23(5).
50. Majors RE, Raynie D. The greening of the chromatography laboratory. *LC-GC N am*. 2011;29(2):118-134.
51. Azevedo CMG, Afonso CMM, Pinto MMM. Routes to xanthones: an update on the synthetic approaches. *Curr Org Chem*. 2012;16(23):2818-2867.
52. Sousa ME, Pinto MMM. Synthesis of xanthones: an overview. *Curr Med Chem*. 2005;12(21):2447-2479.
53. Gales L, Damas AM. Xanthones—a structural perspective. *Curr Med Chem*. 2005;12(21):2499-2515.

SUPPORTING INFORMATION

Additional supporting information may be found online in the Supporting Information section at the end of the article.

How to cite this article: Phyo Y'Z, Teixeira J, Tiritan ME, et al. New chiral stationary phases for liquid chromatography based on small molecules: Development, enantioresolution evaluation and chiral recognition mechanisms. *Chirality*. 2019;1–17. https://doi.org/10.1002/chir.23142